Available online at www.sciencedirect.com
SCIENCE DIRECT®
ELSEVIER
Earth and Planetary Science Letters 211 (2003) 57–68
EPSL
www.elsevier.com/locate/epsl

Postglacial sealevels on a spherical, self-gravitating viscoelastic earth: effects of lateral viscosity variations in the upper mantle on the inference of viscosity contrasts in the lower mantle

Patrick Wu [a,*], Wouter van der Wal [b]

[a] *Department of Geology and Geophysics, University of Calgary, Calgary, AB, Canada T2N 1N4*
[b] *DEOS, Faculty of Aerospace Engineering, Delft University of Technology, Kluyverweg 1, 2629 HS Delft, The Netherlands*

Received 4 December 2002; received in revised form 31 March 2003; accepted 4 April 2003

Abstract

Previous studies of lateral viscosity variations on postglacial rebound often neglect the spherical shape of the Earth and the self-gravity of the solid earth and oceans. In this paper, the consistent sealevel equation is solved by the coupled Laplace–finite element method for a spherical, self-gravitating incompressible Maxwell earth. It confirms the importance of self-gravity in the oceans on sealevel computation near the ice margin where the data are most sensitive to the existence of lateral variations in lithospheric thickness and asthenospheric viscosity. The effects of lateral variations in lower mantle viscosity, asthenospheric viscosity and lithospheric thickness are investigated. This paper confirms the finding of earlier investigations. The combined effect of lateral viscosity variations in the lower mantle with reverse viscosity contrasts in the upper mantle is also investigated. For sealevel data near the center of rebound, the effect of lateral viscosity contrast in the lower mantle can be masked by the existence of a reverse lateral viscosity contrasts in the upper mantle. However, this is not the case for sealevel data just outside the ice margin.

Keywords: glacial rebound; sealevels; mantle dynamics; lateral heterogeneity; viscoelasticity

1. Introduction

Recent advances in seismic tomography clearly show that earth properties vary not only in the radial direction, but also laterally. For example, model S20A [1] shows that underneath the North American craton, SH-wave velocity is faster than the surrounding down to about 350 km. However, this fast anomaly overlies a slower anomaly that extends down to about 650 km and below that another fast anomaly exists in the lower mantle. The origin of lateral variations in seismic velocities can be chemical, thermal, non-isotropic prestress [2] or some combination of the above. Because viscosity is thermally activated and creep parameters depend on chemistry, temperature and pressure, lateral variations in seismic velocities also imply lateral viscosity variations. The slower anomaly between 350 and 650 km depth underneath the North American craton implies a lateral viscosity contrast that is opposite (reverse)

* Corresponding author. Tel.: +1-403-220-7855; Fax: +1-403-284-0074.
E-mail address: ppwu@ucalgary.ca (P. Wu).

0012-821X/03/$ – see front matter
doi:10.1016/S0012-821X(03)00199-7

to that lying above or below. Assuming that lateral structures are due to thermal fluctuation alone, it is estimated that the peak-to-peak lateral viscosity variation in the upper mantle can be as large as two to four orders of magnitude but the lateral variation in the lower mantle is probably smaller [3].

The influence of lateral heterogeneity on postglacial land emergence in and around Fennoscandia has been studied by Sabadini's group [4–9] and Kaufmann et al. [10]. Based on simple axisymmetric ice loads and 2D flat-earth models, these authors concluded that a variation of lithospheric thickness mainly influences the land emergence near the margins of former Fennoscandian ice sheet, whereas the land emergence near the center is relatively insensitive to such variations. The effect of lateral variation in asthenospheric viscosity is slightly larger than that of lithospheric thickness variations, and is best resolved by sealevel data near the ice margin.

Recent studies that use more realistic 3D ice models in the Barents Sea or Fennoscandia with a 3D flat-earth model and real data [11–13] or synthetic data [14] also arrived at similar conclusions.

The influence of lateral density variations in the mantle and lateral viscosity variations in the lower mantle have been studied by Wu et al. [15]. Based on 2D flat-earth models, they found that the effect of lateral density variations is too small to be resolved by the uncertainties of the sealevel data. On the other hand, the effects of lateral viscosity variation in the lower mantle can be quite large even for sealevel sites near the center of rebound in Laurentia.

So far, flat-earth models have been used in all the above studies, and the spherical shape of the Earth and the self-gravitation of the solid earth and its oceans are neglected. However, for large ice sheets like the Laurentide ice sheet, sphericity becomes important. In addition, Farrell and Clark [16] have shown that the effect of gravitational self-consistency on the relative sealevel is significant near the ice margin (see also Section 4). Because these marginal sites are also sensitive to lateral heterogeneities, self-gravitation must be included in these studies. Thus, one of the purposes of this paper is to investigate how sphericity and self-gravity affect the conclusions of previous studies. The finite element (FE) method will be used because the conventional linear perturbation method is limited to cases where lateral viscosity variations are small. Moreover, all the harmonics are coupled when lateral heterogeneities are present [17]. However, the inclusion of self-gravity in the FE model is not straightforward, but it has been successfully implemented in the coupled Laplace–FE method (CLFE) [17,18]. Since this new method does not calculate Normal Modes nor Love Number spectrum, the fully consistent sealevel equation has to be adapted to this approach. Section 2 will describe how the fully consistent sealevel equation can be solved with the CLFE method.

Another purpose of this paper is to investigate the effect that a reverse viscosity contrast between 350 and 650 km underneath the North American craton has on the inference of lateral viscosity contrast in the lower mantle. This issue has been brought up by the work of Wu et al. [19] where the influence of lateral and radial heterogeneities on relative sealevels in Laurentia has been studied with realistic ice and earth models. There, the deglacial phase of the ice load was given by ICE4G [20] with two glacial cycles each with a growth period of 90 ka and deglacial period of 10 ka. Ocean loading was assumed to be uniform over the ocean floor with the amplitude given by the ice equivalent water load (see discussion below Eq. 2). Lateral viscosity variation in the 3D flat-earth was obtained by scaling the SH velocity anomalies in tomography model S20A [1] according to Ivins and Sammis [3] with the temperature profile of Leitch and Yuen [21] for whole mantle convection and the assumption that lateral variations in chemical composition can be neglected ($B = 1$). The radially averaged background viscosity profile R1 was a simplified version of model VM2 [20]. Fig. 1 is reproduced from that study and shows the comparison between the predictions of the reference model R1 (with no lateral heterogeneity) and model S20 (with both radial and lateral viscosity variations). In view of the earlier results of Wu et al. [15], it was surprising to find that the difference between R1 and S20

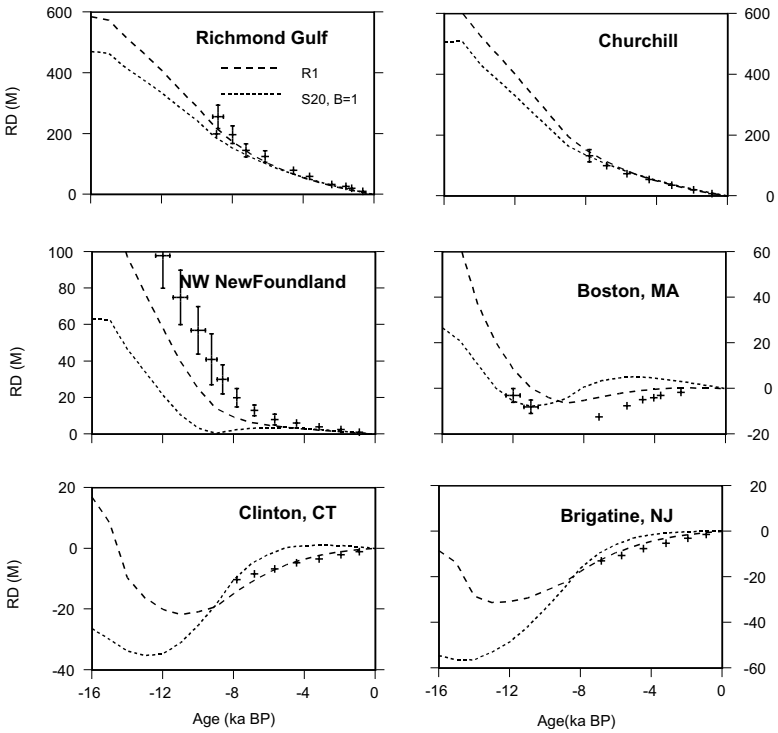

Fig. 1. Relative sealevel data for six North American sites are compared with the predictions of a laterally homogeneous reference model R1 and laterally heterogeneous model S20 (see text for details). Reproduced from Wu et al. [19].

curves is small near the center of rebound (Richmond Gulf and Churchill) despite the existence of a moderate lateral change in lower mantle viscosity in model S20.

Several questions were raised: Firstly, is there a problem with the 3D model or is this due to a difference between 2D and 3D modeling? Secondly, is this because the lateral viscosity contrast in the lower mantle is not large enough? (Lateral viscosity contrast in the lower mantle of model S20 is a factor of 20 less than that used by Wu et al. [15].) Thirdly, is this due to the existence of a reverse lateral viscosity contrast between 350 and 650 km depth? Finally, how will the inclusion of the spherical shape of the earth and self-gravity in the solid earth and the ocean affect these results? (The last question is also relevant to the sealevel sites in Fig. 1 that lie near and outside the ice margin – NW Newfoundland, Boston, Clinton and Brigantine. There, model S20 tends to produce a small land emergence during the last 8 ka, which is not observed. This predicted land emergence might be due to the combined effects of early removal of ice near the margin and channel flow induced by the low viscosities in the laterally heterogeneous asthenosphere or upper mantle. However, uncertainty due to the neglect of the fully consistent sealevel equation may also make the result dubious.)

To answer these questions, we shall continue to use simple axisymmetric ice and earth models because interpretation is simpler and complications due to realistic 3D ice and earth models can be avoided. Furthermore, if the reduced effect shown in relative sealevel predictions near the center of rebound is also present in simple models, then the first question in the last paragraph can be answered. With this simple model, it is also easier to answer the second and third questions by changing the lateral viscosity contrast in the lower mantle and removing the reverse viscosity contrast in the upper mantle.

The outline of this paper is as follows. First, the new method to compute consistent sealevels with

the FE method is briefly reviewed and its validity is demonstrated. Next, the ice and earth model is described. Then, the effect of the gravitationally consistent sealevel equation on relative sealevel computation is briefly reviewed. Following that, the effects of lateral variations in lithospheric thickness, lateral asthenospheric and lower mantle viscosity variations are investigated for this spherical self-gravitating model. Finally, the effects of reverse lateral viscosity variations in the upper mantle are presented.

2. Sealevel computation and its validation

It is well known that tide-gauge and relative sealevel data are not determined with respect to a fixed radius $r = a$. The meter stick for measuring sealevel change is attached to the Earth's solid surface which is displaced by $U(\theta, \psi, t)$ in the radial direction. Thus, the relative motion between the equilibrium ocean surface and the Earth's solid surface is [16,22–26,28–34]:

$$S(\theta, \psi, t) = [\phi(\theta, \psi, t)/g - U(\theta, \psi, t) + c(t)]O(\theta, \psi, t) \quad (1)$$

where $\phi(\theta, \psi, t)$ is the perturbation in potential caused by the redistribution of the external (e.g. ice and water) and internal mass (due to the flow of mantle rocks); g is the surface gravity; $O(\theta, \psi, t)$ is the time dependent ocean function and $c(t)$ is a time dependent quantity required to conserve mass and is given by [16,22–26,28–34]:

$$c(t) = -\frac{M_I(t)}{\rho_w A_o} - \frac{1}{A_o}\left\langle \frac{\phi}{g} - U \right\rangle_o \quad (2)$$

Here A_o is the area of the ocean basins, ρ_w is the density of water, $M_I(t)$ is the mass loss history of the ice at time t and $\langle\ \rangle_o$ represents integration over the ocean basins. The first term on the right of Eq. 2 is the ice-equivalent sealevel. With our new CLFE Method, $U(\theta, \psi, t)$ and $\phi(\theta, \psi, t)$ are computed iteratively using the FE method coupled to Laplace's equation. This FE method is different from the finite disc method used by Clark et al. [24], Wu and Peltier [25], and Tushingham and Peltier [26], where the loads are represented by disc loads. The finite disc method is inadequate since some disc loads overlap each other while others have gaps between them. However, this is not the case with the FE method. Furthermore, the CLFE method does not involve the Normal Mode computation of Love Numbers or Greens Functions. Due to the symmetry of the current problem, an axisymmetric FE grid is used. The grid consists of 18 layers in the mantle (finer layering near the top and coarsening in the lower mantle), each layer consists of 360 elements along the colatitude giving spatial resolutions of 0.5°. The details of the CLFE method can be found in [27].

Recent investigations of the relative sealevel equation include the effect of time dependent ocean margin, near-field water influx and earth rotation [22,28–31]. However, these effects will be neglected in this paper.

Validity of the CLFE method is shown in Fig. 2, where the results of this method are compared with those computed with the pseudo-spectral method [32]. The results of the latter method are obtained from the pseudo-spectral sealevel program coded by G. Di Donato [33] and benchmarked with J.X. Mitrovica's program. The load considered is a 15° uniform disc load (2446 m of ice giving a pressure of 24 MPa) with complemen-

Table 1
Elastic structure of model SG5

Layer	Radius of the top (km)	Density (kg m^{-3})	Rigidity (G Pa)	Gravity (m s^{-2})
Lithosphere	6 371	4 120	73	9.71
Upper mantle	6 271	4,120	95	9.66
Transition zone	5 950	4 220	110	9.57
Lower mantle	5 700	4 508	200	9.51
Core	3 480	10 925	0	10.62

tary ocean. The ice load is put on the north pole of a self-gravitating incompressible spherical earth which consists of a 100-km-thick lithosphere overlying a uniform 10^{21} Pa s viscoelastic mantle and an inviscid fluid core. Because the surface ice and water mass is conserved, the $n=0$ harmonic of the load vanishes. Associated with the ice and water load is the $n=1$ load component which produces rigid shifts in the center of mass [34]. Since the rigid shift is not of interest here, the $n=1$ component of the load has been removed. For this earth and ice model, the pseudo-spectral method summed harmonic contributions up to degree 128. In the CLFE method, Laplace's equation is solved with harmonics up to degree 180, but the load spectrum is tapered with a cosine filter above degree 120 to reduce Gibbs effect at the center. Due to the truncation of the higher harmonics, Gibbs effect becomes severe near the edge of the sharp-corner load even after the spectrum has been tapered. This effect is especially important for the calculation of the potential perturbation or geoid anomaly, but is less severe in the radial displacement because of the presence of the elastic lithosphere.

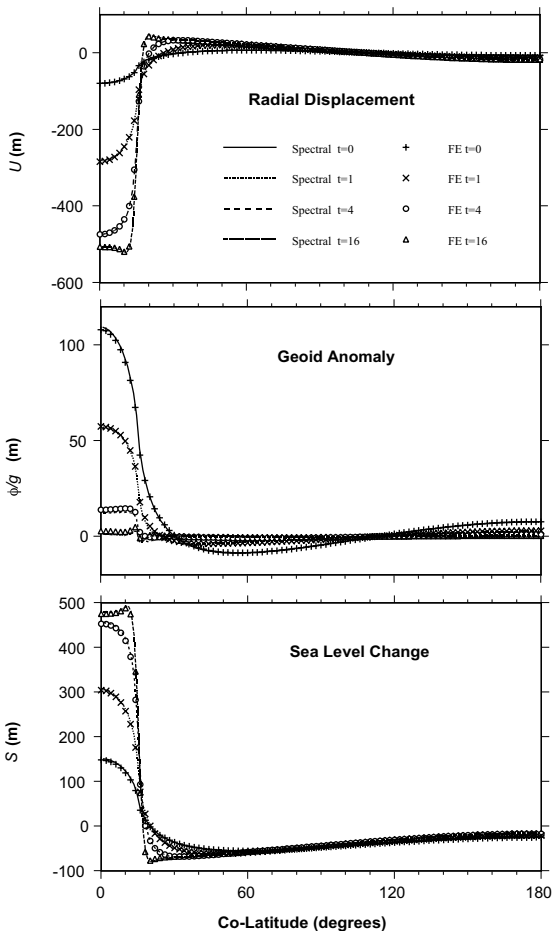

Fig. 2. Evolution of the surface radial displacement, geoid anomaly and sealevel change due to Heaviside loading of a 15° uniform disc load. The lines are predictions of the pseudo-spectral method. These are compared with the results of the CLFE method (symbols).

The evolution of the surface displacement in the radial direction $U(\theta, t)$, the geoid anomaly $\phi(\theta, t)/g$ and the sealevel change $S(\theta, t)$ are computed and plotted in Fig. 2. Although no actual sealevel change occurs on land, Eq. 1 is also applied over the ice to give the plot in Fig. 2. The symbols are the results of the CLFE method while the lines are those computed with the pseudo-spectral method. Despite their vast differences in approach, Fig. 2 shows excellent agreement between them. The difference in $S(\theta, t)$ is below 3% except near the edge of the load where Gibbs effect becomes important.

Inspection of Fig. 2 also shows that the Earth's surface sinks continuously underneath the Heaviside disc load while the geoid anomaly decreases in amplitude when the load becomes increasingly compensated. Thus, the geoid anomaly has a significant contribution to the sealevel change for small time t, but its contribution decreases at large time t – when the sealevel change is given by the negative of the radial displacement.

3. Ice and earth models for the study of lateral heterogeneity

To avoid Gibbs effect, the profile of the disc load is taken to be elliptical for the rest of this paper. Here ice thickness H at colatitude θ and time t is given by:

$$H(\theta, t) = H_{\mathrm{MAX}}(t)\sqrt{1-(\theta/\theta_{\mathrm{MAX}})^2} \qquad (3)$$

$$H_{\mathrm{MAX}}(t) =$$

$$\begin{cases} H_0\dfrac{t+106}{90} & -106\ \text{ka BP} \le t \le -16\ \text{ka BP} \\ H_0\dfrac{(-6-t)}{10} & -16\ \text{ka BP} \le t \le -6\ \text{ka BP} \\ 0 & -6\ \text{ka BP} < t < 0\ \text{ka BP} \end{cases} \quad (4)$$

where the peak thickness is $H_0 = 3663$ m and the angular radius of the disc load $\theta_{\mathrm{MAX}} = 15°$. Thus, as the ice sheet grows during the 90-ka glacial period and decays in the 10-ka deglacial period, the ice margin remains constant. For simplicity, the ocean is again taken to be complementary to the ice.

The elastic structure of all earth models is given by model SG5 (Table 1). For the viscosity structure, two types of models are considered. In type A models, lithospheric thickness is uniformly 100 km thick and lateral heterogeneity only exists in the mantle (see Fig. 3a). The viscosities of the various areas in Fig. 3a are given in Table 2a. In type B models, there is lateral variation in lithospheric thickness: 150-km-thick craton under the center of the ice sheet; 4° within the ice margin it starts to decrease to 50 km at 4° outside. Beyond that, lithospheric thickness remains at 50 km under the rest of the ocean (see Fig. 3b). Tables 2a,b list all the viscosity models considered in this paper. The first letter in the names of these models refers to either type A or type B model. The other letters in the name refer to the different structures: the letter U means uniform 1×10^{21} Pa s mantle, HLM refers to a high viscosity lower mantle, LM is for lateral variation in lower mantle viscosity and AS refers to lateral variation in asthenospheric viscosity. Finally, model BNA has both lateral and radial viscosity variations and their values are inferred from seismic tomography model S20A [1] under North America. The only difference between BNA1 and BNA2 is that the

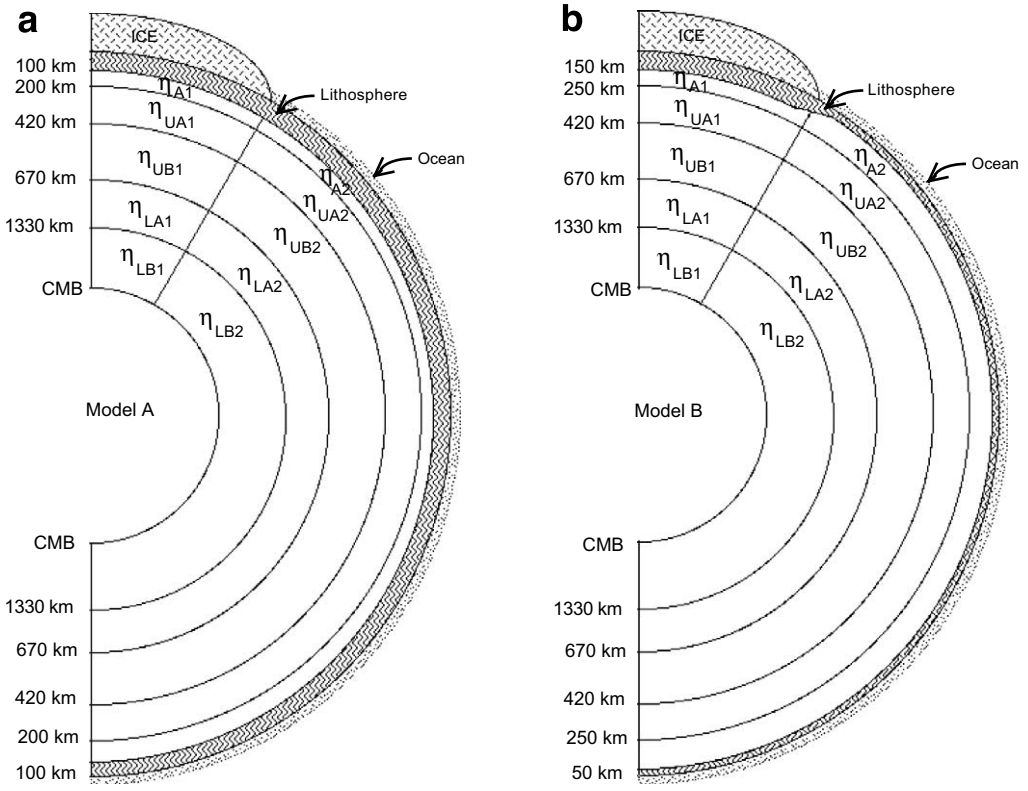

Fig. 3. Schematic diagrams of spherical earth models A and B. The former has a uniformly 100-km-thick lithosphere whereas the latter has a 150-km-thick lithospheric under the load but a 50-km oceanic lithosphere outside.

Table 2a
Viscosity values (Pa s) in earth model A with uniform lithospheric thickness

	AU	AHLM	ALM1	ALM2	AAS
$\eta_{A1}:\eta_{A2}$	$1\times10^{21}:1\times10^{21}$	$1\times10^{21}:1\times10^{21}$	$1\times10^{21}:1\times10^{21}$	$1\times10^{21}:1\times10^{21}$	$1\times10^{22}:1\times10^{20}$
$\eta_{UA1}:\eta_{UA2}$	$1\times10^{21}:1\times10^{21}$	$1\times10^{21}:1\times10^{21}$	$1\times10^{21}:1\times10^{21}$	$1\times10^{21}:1\times10^{21}$	$1\times10^{21}:1\times10^{21}$
$\eta_{UB1}:\eta_{UB2}$	$1\times10^{21}:1\times10^{21}$	$1\times10^{21}:1\times10^{21}$	$1\times10^{21}:1\times10^{21}$	$1\times10^{21}:1\times10^{21}$	$1\times10^{21}:1\times10^{21}$
$\eta_{LA1}:\eta_{LA2}$	$1\times10^{21}:1\times10^{21}$	$1\times10^{22}:1\times10^{22}$	$1\times10^{21}:1\times10^{22}$	$1\times10^{22}:1\times10^{21}$	$1\times10^{21}:1\times10^{21}$
$\eta_{LB1}:\eta_{LB2}$	$1\times10^{21}:1\times10^{21}$	$1\times10^{22}:1\times10^{22}$	$1\times10^{21}:1\times10^{22}$	$1\times10^{22}:1\times10^{21}$	$1\times10^{21}:1\times10^{21}$

latter has a larger lateral viscosity contrast in the lower mantle. BNA3 is the same as BNA2 except there is no reversal of viscosity contrast in the upper mantle. Model BR1 has the same viscosity profile as the reference model R1 of Wu et al. [19] below the lithosphere.

4. Effects of consistent sealevels

One of the improvements of this work is that self-gravitating spherical earth models are used. Another improvement is that the consistent sealevel equation is solved rather than using a first order approximation of Eq. 1, where it is assumed that the melted ice water gets distributed uniformly over the oceans, so that the sealevel change becomes:

$$S_l(\theta,\ \psi,\ t) = [U_l(\theta,\ \psi,\ t) + c_l(t)]O(\theta,\ \psi,\ t) \quad (5)$$

where $c_l(t) = -(M_l(t)/\rho_w A_o)$ is the ice-equivalent sealevel and U_l is the radial displacement if the ocean load is just due to $c_l(t)$. If no water enters into the ocean after the end of deglaciation (i.e. neglecting current melting in Greenland, Antarctica or alpine glaciers), then the relative change in S_l just gives relative displacement curves. The purpose of this section is to show that such an approximation is especially poor near the ice margin. A similar investigation has been carried out in figure 4 of Wu and Peltier [25]. However, in that paper, the radial displacement was computed with an ocean load that satisfies the consistent sealevel equation (i.e. using U instead of U_l in Eq. 5).

Fig. 4 is computed for earth model AU with the elliptic ice model described in Section 3. The predicted relative sealevel curves at four sites (0°, 14°, 16° and 20° from the load center) are plotted. Superimposed on these are relative sealevel observations in Richmond Gulf, NW Newfoundland, Boston and Brigantine respectively. Because the ice model used is very simple and does not allow for the migration of the ice margin, the predicted curves are not expected to fit these observations. Thus, the sole purpose of displaying the observations is to see if the difference between S and the S_l approximation is resolvable by the data.

First of all, the difference between $S(\theta,\ t)$ and $S_0 = -U(\theta,\ t)+c(t)$ gives the contribution of the geoid anomaly to relative sealevels. When this difference is plotted (not shown), it is found that the value is about 30 m at −16 ka BP but decreases to less than 1 m after the end of deglaciation at −6 ka BP. This shows that the contribution of the geoid anomalies can be neglected only if we are interested in sealevel data within the last 6–8 ka. Secondly, the difference between the spatially independent quantities for mass conservation $c(t)$ and $c_l(t)$ is about 10 m at 16 ka BP

Table 2b
Viscosity values (Pa s) in earth model B with heterogeneous lithosphere

	BU	BAS	BNA1	BNA2	BNA3	BR1
$\eta_{A1}:\eta_{A2}$	$1\times10^{21}:1\times10^{21}$	$1\times10^{22}:1\times10^{20}$	$1\times10^{23}:1\times10^{20}$	$1\times10^{23}:1\times10^{20}$	$1\times10^{23}:1\times10^{20}$	$6\times10^{20}:6\times10^{20}$
$\eta_{UA1}:\eta_{UA2}$	$1\times10^{21}:1\times10^{21}$	$1\times10^{21}:1\times10^{21}$	$1\times10^{21}:5\times10^{20}$	$1\times10^{21}:5\times10^{20}$	$1\times10^{21}:5\times10^{20}$	$6\times10^{20}:6\times10^{20}$
$\eta_{UB1}:\eta_{UB2}$	$1\times10^{21}:1\times10^{21}$	$1\times10^{21}:1\times10^{21}$	$1\times10^{20}:5\times10^{20}$	$1\times10^{20}:5\times10^{20}$	$5\times10^{20}:5\times10^{20}$	$6\times10^{20}:6\times10^{20}$
$\eta_{LA1}:\eta_{LA2}$	$1\times10^{21}:1\times10^{21}$	$1\times10^{21}:1\times10^{21}$	$5\times10^{21}:1\times10^{21}$	$1\times10^{22}:1\times10^{21}$	$1\times10^{22}:1\times10^{21}$	$1.6\times10^{21}:1.6\times10^{21}$
$\eta_{LB1}:\eta_{LB2}$	$1\times10^{21}:1\times10^{21}$	$1\times10^{21}:1\times10^{21}$	$5\times10^{21}:1\times10^{21}$	$1\times10^{22}:1\times10^{21}$	$1\times10^{22}:1\times10^{21}$	$3\times10^{21}:3\times10^{21}$

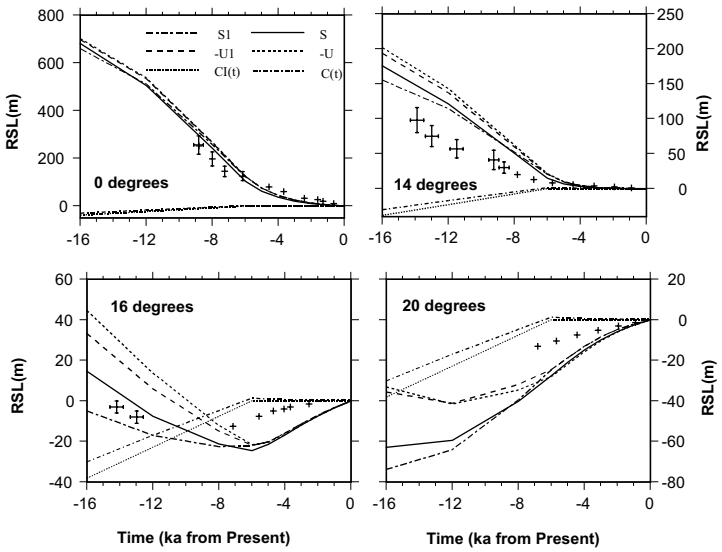

Fig. 4. Comparing the contribution of the different terms in the consistent sealevel equation (S, $-U$ and $C(t)$) with that of the first order approximation (S_1, $-U_1$ and $C_1(t)$).

(see Fig. 4), but decreases to about 1.4 m at the end of deglaciation when $c(t)$ decreases to zero while $c_1(t)$ remains at zero up to the present. Thirdly, the difference between U and U_1 (Fig. 4) is large, especially near the ice margin and for ancient beaches older than about 8 ka BP. The same can be said about the difference between S and S_1 (Fig. 4). Since ancient sealevel data (older than about 6 ka BP) just around the ice margin are most sensitive to the lateral lithospheric thickness and asthenospheric viscosity variations [4,10,15] (also Fig. 5) future investigations of lateral heterogeneities should employ Eq. 1 rather than Eq. 5.

5. Effects of lateral viscosity variations

First, let us investigate the effects of lateral lithospheric thickness and asthenospheric viscosity variations underneath an ice load with size comparable to the Laurentian ice sheet. Similar effects for a smaller ice load with size comparable to the Fennoscandian ice on a non-self-gravitating flat earth have been studied with relative displacements [4,10,15]. It was found that for the smaller load, these effects are too small to be resolved by the observations at the load center (unless viscosity variation in the asthenosphere has a long wavelength). However, around the ice margin, the effects of lateral variations in lithospheric thickness and asthenospheric viscosity are discernible by the data. Fig. 5 shows these effects on relative sealevels for the 15° load on a spherical self-gravitating earth. In this figure, the predicted relative sealevel curves for models AU, BU, BAS and AAS are compared at four sites (0°, 14°, 16° and 20° from the load center). Again, the sole purpose of displaying the observations is to see how well the data can discriminate between different earth models.

Comparing the curves for model AU and BU confirms that the effect of lateral variation in lithospheric thickness alone is too small to be resolved by the observations inside the ice sheet or at the far field. This effect is only resolvable for sites just outside the ice margin.

Comparing the curves for models AU and AAS in Fig. 5 shows that the effect of lateral asthenospheric viscosity variation is larger than the effect of lateral lithospheric variation, but is still unresolvable by the data except for sites just outside the ice margin [10,13].

The effect of combined lateral lithospheric and

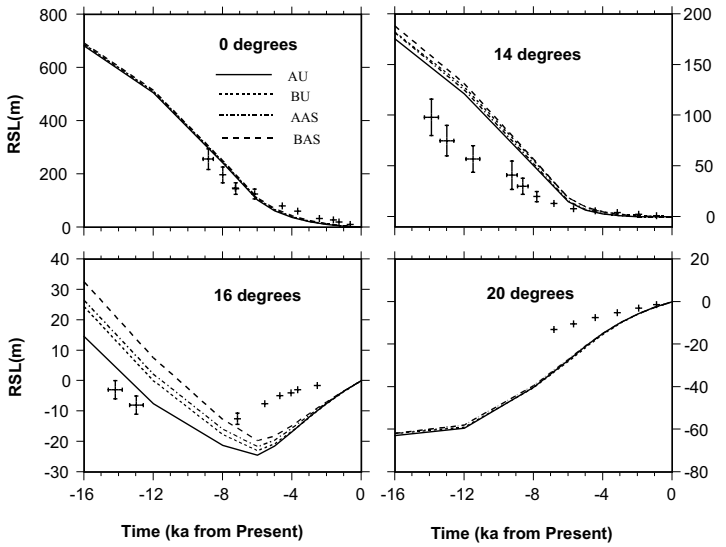

Fig. 5. Comparing the relative sealevel (RSL) predictions of models AU, BU, AAS and BAS (Tables 2a,b) at four different sites from the 15° elliptical disc load.

asthenospheric viscosity variations is shown by comparing models BAS, AU, AAS and BU in Fig. 5. Again, the combined effect is slightly larger than that due to lateral lithospheric or asthenospheric viscosity variation alone. However, the difference is again resolvable only at sites just outside the ice margin.

Next, let us study the effect of lateral viscosity variation in the lower mantle. Unlike the results for lateral variations in lithospheric thickness or asthenospheric viscosity, Wu et al. [15] have shown that the effect of lateral viscosity variation in the lower mantle is large even for relative sealevel sites away from the Laurentian ice margin. However, in that study, a flat non-self-gravitating earth was used. Also, relative displacement curves instead of relative sealevels are computed. Here, we wish to see if the introduction of self-gravitation, sphericity and the self-consistent sealevels would alter those conclusions. Inspection of Fig. 6 shows that near the center of the load, the predictions of models AU and ALM1 are closer together than those of models AHLM and ALM2. This is because the viscosities of the upper and lower mantle directly below the load center are the same between models AU and ALM1. The same can be said for models AHLM and ALM2. However, the difference in the relative sealevel amplitudes between AU and ALM1 or AHLM and ALM2 at times earlier than 8 ka BP means that the sealevel curves are also sensitive to lower mantle viscosities 15° away. The difference between these two sets of curves at times earlier than 8 ka BP is large enough to be discriminated by the sealevel data near the center. However, it is interesting to note that near the ice margin (14° and 16°), model ALM1 is closer to AHLM, while model ALM2 is closer to AU. At 14°, the differences between models ALM1 and AHLM or between ALM2 and AU are too small to be resolved by the data. However, the difference between the two sets of curves is large enough to be resolved. At 16° and 20°, the difference between all these curves is also large enough to be discriminated by the observations. Thus, Fig. 6 confirms the earlier finding [15] that lateral viscosity variations in the lower mantle can be resolved by the relative sealevel data within and outside the Laurentian ice margin.

Finally, the combined effects of lateral viscosity variations in the lower mantle and a reverse viscosity contrast in the upper mantle are shown in Fig. 7. The viscosity structures of models BNA1, BNA2 and BNA3 are given in Table 2b. Fig. 7 shows that for sealevel sites near the center of rebound, the difference between model BNA1

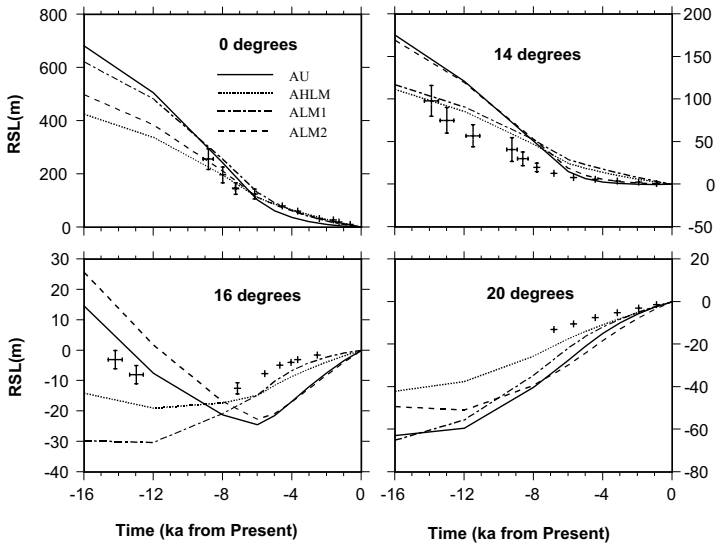

Fig. 6. Same as Fig. 5, except for models AU, AHLM, ALM1 and ALM2 (Tables 2a,b).

and the laterally homogeneous reference model BR1 is much smaller than the difference between models ALM2 and AU in Fig. 6. To test if this is due to the small lateral viscosity contrast in the lower mantle, model BNA2 is constructed so that the lateral viscosity contrast in the lower mantle is the same as that in model ALM2. Fig. 7 shows that the difference between models BNA2 and BR1 is now larger near the center of rebound, but still not as large as the difference between models ALM2 and AU (Fig. 6). If we now remove the reverse viscosity contrast in the transition zone (model BNA3), then we see that the difference between BR1 and BNA3 near the center of the load is almost as large as that between AU and ALM2 (Fig. 6). At the other sites (14°,

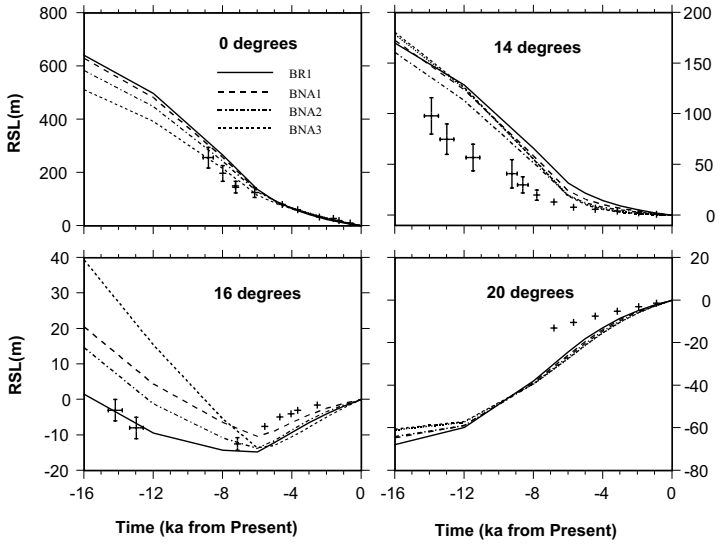

Fig. 7. Same as Fig. 5, except for models BR1, BNA1, BNA2 and BNA3 (Tables 2a,b).

16° and 20°), the difference is also comparable to that predicted in Fig. 6. (These differences are only 'almost' as large as that predicted in Fig. 6 because of the lateral viscosity contrast in the shallow part of BNA3.) Thus, in the presence of a reverse lateral viscosity contrast in the upper mantle, sealevel data near the center of rebound cannot detect the lateral viscosity contrasts in the lower mantle. For sealevel data just outside the ice margin, the influence of lateral viscosity contrasts in the lower mantle is reduced but is still discernible.

6. Conclusions

Inclusion of self-gravity in the oceans of a spherical viscoelastic earth significantly affects the sealevel computation near the ice margin but the effect is not large enough to alter the conclusions of earlier studies with non-self-gravitating flat-earth models. The presence of a reverse viscosity contrast in the upper mantle can mask the effect of lateral viscosity variations in the lower mantle, as far as relative sealevel data near the center of rebound are concerned. The effects of lateral viscosity variations on radial and tangential velocities and the geoid rate of change are also large, but that is the subject of the next paper [35].

Acknowledgements

We thank Drs. Shijie Zhong, Bert Vermeersen, Scott King and an anonymous reviewer for their constructive reviews. The FE calculation was performed with the ABAQUS package from Hibbitt, Karlsson and Sorensen Inc. This research is supported by an Operating Grant from NSERC of Canada to P.W.*[SK]*

References

[1] G. Ekstrom, A. Dziewonski, The unique anisotropy of the Pacific upper mantle, Nature 394 (1998) 168–172.
[2] [2] F.A. Dahlen, J. Tromp, Theoretical Global Seismology, Princeton University Press, 1998.
[3] E.R. Ivins, C.G. Sammis, On lateral viscosity contrast in the mantle and the rheology of low-frequency geodynamics, Geophys. J. Int. 123 (1995) 305–322.
[4] R. Sabadini, D.A. Yuen, M. Portney, The effects of upper mantle lateral heterogeneities on postglacial rebound, Geophys. Res. Lett. 13 (1986) 337–340.
[5] R. Sabadini, P. Gasperini, Glacial isostasy and the interplay between upper and lower mantle lateral viscosity heterogeneities, Geophys. Res. Lett. 16 (1989) 429–432.
[6] P. Gasperini, R. Sabadini, Lateral heterogeneities in mantle viscosity and post-glacial rebound, Geophys. J. 98 (1989) 413–428.
[7] P. Gasperini, D.A. Yuen, R. Sabadini, Effects of lateral viscosity variations on postglacial rebound: implications for recent sea-level trends, Geophys. Res. Lett. 17 (1990) 5–8.
[8] P. Gasperini, R. Sabadini, D.A. Yuen, Deep continental roots: the effects of lateral variations of viscosity on postglacial rebound, in: R. Sabadini, K. Lambeck, E. Boschi (Eds.), Glacial Isostasy, Sea Level and Mantle Rheology, Kluwer Academic Publishers, Dordrecht, 1991, pp. 21–32.
[9] C. Giunchi, G. Spada, R. Sabadini, Lateral viscosity variations and postglacial rebound: effects on present-day VLBI baseline deformations, Geophys. Res. Lett. 24 (1997) 13–16.
[10] G. Kaufmann, P. Wu, D. Wolf, Some effects of lateral heterogeneities in the upper mantle on postglacial land uplift close to continental margins, Geophys. J. Int. 128 (1997) 175–187.
[11] G. Kaufmann, P. Wu, Lateral asthenospheric viscosity variations and postglacial rebound: a case study for the Barents Sea, Geophys. Res. Lett. 25 (1998) 1963–1966.
[12] G. Kaufmann, P. Wu, G. Li, Glacial isostatic adjustment in Fennoscandia for a laterally heterogeneous Earth, Geophys. J. Int. 143 (2000) 262–273.
[13] G. Kaufmann, P. Wu, Glacial isostatic adjustment on a three-dimensional earth: examples from Fennoscandia and the Barents Sea, in: J.X. Mitrovica, L.L.A. Vermeersen (Eds.), Sea-level, Crustal Deformation, Gravity and Rotation, AGU Geodynamics Series, 2002, pp. 293–309.
[14] G. Kaufmann, P. Wu, Glacial isostatic adjustment in Fennoscandia with a three dimensional viscosity structure as an inverse problem, Earth Planet. Sci. Lett. 197 (2002) 1–10.
[15] P. Wu, Z. Ni, G. Kaufmann, Postglacial rebound with lateral heterogeneities: from 2D to 3D modeling. in: P.Wu (Ed.), Dynamics of the Ice Age Earth: A Modern Perspective, Trans Tech Publications, Zurich, 1998, pp. 557–582.
[16] W.E. Farrell, J.A. Clark, On postglacial sea level, Geophys. J. R. Astron. Soc. 46 (1976) 647–667.
[17] P. Wu, Mode coupling in a viscoelastic self-gravitating spherical earth induced by axisymmetric loads and lateral viscosity variations, Earth Planet. Sci. Lett. 202 (2002) 49–60.
[18] P. Wu, Effects of nonlinear rheology on degree 2 harmon-

ic deformation in a spherical self-gravitating earth, Geophys. Res. Lett. 29 (2002) 10.1029/2001GL014109.
[19] P. Wu, J. Wahr, W.R. Peltier, Thermally induced lateral viscosity variations and postglacial rebound: implications for relative sea levels in Laurentia, IUGG 99 Birmingham Abstracts, 1999, p. A61.
[20] W.R. Peltier, Ice age paleotopography, Science 265 (1994) 195–201.
[21] A.M. Leitch, D.A. Yuen, Internal heating and thermal constraints on the mantle, Geophys. Res. Lett. 16 (1989) 1407–1410.
[22] W.R. Peltier, Postglacial variations in the level of the sea: implications for climate dynamics and solid-earth geophysics, Rev. Geophys. 36 (1998) 603–689.
[23] G.A. Milne, J.X. Mitrovica, D.P. Schrag, Estimating past continental ice volume from sea-level data, Quat. Sci. Rev. 21 (2002) 361–376.
[24] J.A. Clark, W.E. Farrell, W.R. Peltier, Global changes in postglacial sea level: a numerical calculation, Quat. Res. 9 (1978) 265–287.
[25] P. Wu, W.R. Peltier, Glacial isostatic adjustment and the free air gravity anomaly as a constraint on deep mantle viscosity, Geophys. J. R. Astron. Soc. 74 (1983) 377–450.
[26] A.M. Tushingham, W.R. Peltier, Ice-3G: a new global model of late Pleistocene deglaciation based upon geophysical predictions of post-glacial relative sea-level change, J. Geophys. Res. 96 (1991) 4497–4523.
[27] P. Wu, Using commercial finite element packages for the study of earth deformations, sea levels and the state of stress, submitted.
[28] P. Johnston, The effect of spatially non-uniform water loads on predictions of sea-level change, Geophys. J. Int. 114 (1993) 615–634.
[29] G.A. Milne, Refining models of the glacial isostatic adjustment process, Ph.D. thesis, University of Toronto, Toronto, Canada, 1998, 124 pp.
[30] G.A. Milne, J.X. Mitrovica, The influence of of a time-dependent ocean-continent geometry on predictions of post-glacial sea level change in Australia and New Zealand, Geophys. Res. Lett. 25 (1998) 793–796.
[31] G.A. Milne, J.X. Mitrovica, Postglacial sealevel change on a rotating Earth, Geophys. J. Int. 133 (1998) 1–19.
[32] J.X. Mitrovica, W.R. Peltier, On postglacial geoid subsidence over the equatorial oceans, J. Geophys. Res. 96 (1991) 20053–20071.
[33] G. di Donato, L.L.A. Vermeersen, R. Sabadini, Sea-level changes, geoid and gravity anomalies due to Pleistocene deglaciation by means of multilayered, analytical Earth models, Tectonophysics 320 (2000) 409–418.
[34] W.E. Farrell, Deformation of the earth by surface loads, Rev. Geophys. Space Phys. 10 (1972) 761–797.
[35] P. Wu, Postglacial induced surface motions, sealevels and geoid rate on a spherical, self-gravitating laterally heterogeneous earth, submitted.